J Therm Anal Calorim (2016) 123:91–103
DOI 10.1007/s10973-015-4956-7

Synthesis, characterization and thermal behavior of solid state of some mefenamate of trivalent lanthanides (La, Ce, Pr and Nd)

Francisco X. Campos[1,2] · André L. C. S. Nascimento[1] · Tiago A. D. Colman[1] · Diogo A. Gálico[4] · Oswaldo Treu-Filho[1] · Flávio J. Caires[3] · Adriano B. Siqueira[5] · Massao Ionashiro[1]

Received: 28 May 2015 / Accepted: 2 August 2015 / Published online: 14 August 2015

Abstract Solid-state $Ln(Mef)_3$ compounds, where Ln stands for some trivalent lanthanides (La, Ce, Pr and Nd) and Mef is the mefenamate ($C_{15}H_{14}NO_2^-$) ligand, were synthesized. The characterization and thermal and spectroscopic study of the compounds were performed using elemental analysis, complexometry, image analysis by field emission gun, simultaneous thermogravimetry and differential scanning calorimetry coupled to Fourier transform infrared spectroscopy, X-ray diffractometry, near-infrared and mid-infrared spectroscopy. All the analyses showed that the compounds were obtained in the anhydrous state. The thermoanalytical results showed that the stability and thermal behavior were markedly influenced by the atmosphere used. Moreover, the curves show that the thermal decomposition takes place in two or three steps, with the formation of lanthanide oxide (La_2O_3, CeO_2, Pr_6O_{11} and Nd_2O_3), as the final residue. Furthermore, the theoretical and experimental spectroscopic data suggested the possible modes of coordination of the ligand with the metals. The DR spectra provided information about the ligand absorption bands and the *f–f* transitions of Nd^{3+} and Pr^{3+} ions.

Keywords Mefenamate · Lanthanides · Thermal analysis · Spectroscopy · DFT

Introduction

Mefenamic acid, (2[(2,3-dimethyl-phenyl) amino] benzoic acid), crystalline solid sparingly soluble in water, with molecular formula $C_{15}H_{15}NO_2$ is an nonsteroidal anti-inflammatory drug (NSAID) used to treat pain related to dysmenorrhea and rheumatoid arthritis. Its therapeutic activity is related to the inhibition of prostaglandin biosynthesis by the competitive interaction with the arachidonic acid and complex or by the ending of the activity of free radicals that interfere with the initiation of the synthesis of cyclooxygenase [1, 2].

Several studies have been conducted with nonsteroidal anti-inflammatory drugs which have demonstrated that the action of the precursor improves with the association of metals with very different objectives [1–5]. It should be mentioned that when mefenamic acid was combined with metals such as bismuth (III), a compound capable of acting against the leishmaniasis parasite was obtained, which also had low toxicity in relation to infected cells [4]; when mefenamic acid was associated with transition metals such manganese (II), iron (II), cobalt (II), nickel (II), copper (II) and zinc (II), there was an increase in the antioxidant activity of the new compounds compared to the precursor mefenamic acid [1, 5]. Mefenamic acid also improves the ability to bind to DNA, for zinc compound (II) which demonstrates promising anticancer activity potential [3, 5].

Electronic supplementary material The online version of this article (doi:10.1007/s10973-015-4956-7) contains supplementary material, which is available to authorized users.

✉ Flávio J. Caires
caires.flavio@yahoo.com.br

[1] Instituto de Química, UNESP – Univ. Estadual Paulista, Araraquara, SP 14801-970, Brazil

[2] Instituto Federal de Educação, Ciência e Tecnologia de Mato Grosso, Primavera do Leste, MT 78850-000, Brazil

[3] Faculdade de Ciências, UNESP – Campus Bauru, CEP 17033-260 Bauru, SP, Brazil

[4] Instituto de Química, UNICAMP – Univ. Estadual de Campinas, Campinas, SP 13083-970, Brazil

[5] IE/CUVG/Univ. Federal de Mato Grosso, Cuiabá, MT 78060-900, Brazil

The literature contains descriptions of synthesized structures of the mefenamate of transition metals [1], mefenamate studies with solvents which behave as organic binders in the coordination sphere of transition metals [2, 3, 5] and a study of mefenamate structure with Fe(III) associated with chloride or sodium, forming mononuclear and binuclear structures of Fe(III) [7]. In the above-mentioned studies, the authors used various techniques such as elemental analysis (EA), spectroscopy in the infrared region, nuclear magnetic resonance of hydrogen and carbon 13, thermal analysis, X-ray diffraction and complexometry.

In the literature, there is one article that treats the mefenamate compounds of lanthanides [6], in which only the thermal study in a static air atmosphere is described; thus, a more detailed study is missing. Also, in a second stage, studies of luminescence and biological will be carried out, since works with lanthanide complexes with ketoprofen, another NSAID have been synthesized and did not show cytotoxic effects on human cells. Furthermore, some of them showed luminescent properties due to an excellent energy transfer between the ligand and the lanthanide ion [8–10].

Thus, the present paper deals with the preparation of solid-state compounds of some trivalent lanthanides (La, Ce, Pr and Nd) with a mefenamate ligand and investigations using complexometry, EA, TG–DSC–FTIR, X-ray powder diffractometry, diffuse reflectance (DR), near-infrared region (NIR) spectroscopy and image analysis by field emission gun (FEG).

Experimental

Material

Mefenamic acid ($C_{15}H_{15}NO_2$) was obtained from Sigma-Aldrich, and the purity of 99.6 % was determined by DSC [1]. The lanthanides were prepared from the metal oxides (La_2O_3, Nd_2O_3 and Pr_6O_{11}) except cerium, where cerium nitrate $Ce(NO_3)_3{\cdot}6H_2O$ was used; all were obtained from Sigma, with a purity of 99.9 %.

Synthesis

Lanthanide chlorides were prepared from the corresponding metal oxides, except for cerium, by treatment with concentrated hydrochloric acid (Eq. 1). The resulting solutions were evaporated to near dryness to eliminate the excess of hydrochloric acid. The residues were dissolved in distilled water and diluted in order to obtain ca. 0.10 mol L^{-1} solutions, whose pH was adjusted to 5.0 by adding diluted sodium hydroxide or hydrochloric acid solutions. Cerium (III) was used as nitrate, and ca. 0.10 mol L^{-1} aqueous solution of this ion was prepared by direct weighing of the salt.

$$Ln_2O_{3(aq)} + 6HCl_{(aq)} \rightarrow 2\ LnCl_{3(aq)} + 3H_2O_{(l)} \quad (1)$$

An aqueous solution of 0.10 mol L^{-1} sodium mefenamate was prepared by neutralization of aqueous suspension of mefenamic acid with 0.10 mol L^{-1} sodium hydroxide (Eq. 2).

$$C_{15}H_{15}NO_{2(aq)} + NaOH_{(aq)} \rightarrow NaC_{15}H_{14}NO_{2(aq)} + H_2O_{(l)} \quad (2)$$

Solid-state compounds were obtained by slowly adding, with stirring, 150.0 mL of 0.10 mol L^{-1} sodium mefenamate, which was heated to near ebullition with 50.0 mL of the respective 0.10 mol L^{-1} metal ions solutions, which were also heated (Eq. 3). The precipitates were washed with distilled water until chloride or nitrate ions were eliminated. They were then filtered and dried at 50 °C in a forced circulation over for 12 h and maintained in a desiccator over anhydrous calcium chloride.

$$3NaC_{15}H_{14}NO_{2(aq)} + LnCl_{3(aq)} \rightarrow Ln(C_{15}H_{14}NO_2)_3 + 3NaCl_{(l)} \quad (3)$$

Experimental equipment and conditions

The solid-state metal ions, hydration water and mefenamate contents were determined from TG curves. The metal ions were also determined by complexometry using standard EDTA solution, after igniting the compounds to the respective oxides and their dissolution in hydrochloric acid solutions [11, 12].

Carbon, hydrogen and nitrogen contents were determined by microanalytical procedures, with CHN elemental analyzer from Perkin Elmer, model 2400, and also from TG curves.

The elemental composition was also determined by energy-dispersive spectroscopy (EDS) in a X-Max^N analyzer with 20 mm^2 SDD detector from Oxford Instruments and Aztec Energy software package, using a Tescan Lyra dual beam microscope with an FEG electron source.

Simultaneous thermogravimetry and differential scanning calorimetry curves (TG–DSC) were obtained using a STAR^e thermogravimetric analyzer system from Mettler-Toledo. The purge gas had an air and/or N_2 flow of 50 mL min^{-1}. A heating rate of 10 °C min^{-1} was adopted, with samples weighing about 5 mg. Alumina crucibles were used for recording the TG–DSC curves.

The evolved gas analysis (EGA) was performed using a Mettler TG–DSC thermogravimetric analyzer coupled to a FTIR Nicolet spectrophotometer with gas cell and DTGS KBr detector. The furnace and heated gas cell (250 °C) were coupled through a heated (225 °C) 120-cm stainless

steel line transfer with diameter of 3.0 mm, both purged with dry air (50 mL min^{-1}). The FTIR spectra were recorded with 16 scans per spectrum at a resolution of 4 cm^{-1}. (Absorption bands produced by background subtraction by the presence of H_2O around 3800 cm^{-1} and around 1600 cm^{-1} should be disregarded in the analysis of gaseous products formed in this equipment.)

X-ray powder patterns were obtained by using a Bruker AXS D8 Advance X-ray diffractometer employing CuKα radiation (λ = 1.544 Å) and setting of 40 kV and 40 mA.

Diffuse reflectance (DR) spectra were acquired using a Varian Cary 5000 spectrophotometer within the 200–1000 nm range with spectral resolution of 0.5 nm.

Near-infrared spectra (NIR) were collected using a Thermo Scientific Antaris II spectrophotometer by reflectance, within the 1000–2500 nm range.

Mid-infrared spectra (MIR) were run on a Nicolet iS10 Fourier transform infrared spectrophotometer (FTIR), using an ATR accessory with Ge window. The MIR spectra were recorded in the region of 4000–600 cm^{-1} with 32 scans per spectrum at the resolution of 4 cm^{-1}.

The micrographs were acquired using a Tecscan Mira FEG device, with an increase resolution of 30000×. For the acquisition of images, the samples were metallized with a mixture of Au/Pd in Quorum SC 7620 sputter coater.

Computational strategy

In this study, the employed quantum chemical approach to determine the molecular structures was Becke three-parameter hybrid theory [13] using the Lee–Yang–Par (LYP) correlation functional [14]. The basis sets used for the calculations were: [4s] for H (^{2}S) [12], [5s4p] for C (^{3}P), N (^{4}S) and O (^{3}P) [15] and [17s11p7d] for La (^{2}D) [16]. The diffuse functions for the lanthanum atom (^{2}D) were calculated according to the procedure described in Ref. [15], and these values are: αs = 0.00669534, αp = 0.079333735, αd = 0.096432865.

In order to better describe the properties of the compound in the implementation of the calculations, it was necessary to include polarization functions [15–17] for all the atoms of the compound.

The polarization functions were: αp = 0.33353749 for H (^{2}S), αd = 0.72760279, αd = 0.35416230 and αd = 0.36059494 for C (^{3}P), N (^{4}S) and O (^{3}P), respectively, and αf = 0.36935391 for La (^{2}D) atoms. Full details about the wave function used in this study are available upon request to the e-mail address: oswaldo.treu.filho@gmail.com. The role of a basis set is a crucial point in theoretical studies of metal complexes because the description of the configuration of the metal in the complex differs from the neutral state. The molecular calculations in this study were performed using the Gaussian 09 routine [18].

The theoretical infrared spectrum was calculated using a harmonic field [19] based on C_1 symmetry (electronic state ^{1}A). The geometry optimization was computed using the optimized algorithm of Berny [20], and the calculations of vibrational frequencies were also implemented to determine an optimized geometry that constitutes minimum or saddle points. The principal infrared active fundamental mode assignments and descriptions were performed using the GaussView 5.0.2 W graphics routine [21].

Results and discussion

Analytical results

The analytical and thermoanalytical (TG) data are given in Table 1. All data are in excellent agreement, suggesting that the compounds were obtained with excellent purity. These results made it possible to establish the stoichiometry of the compounds, which were in agreement with the general formula $Ln(Mef)_3$, where Ln represents lanthanides and Mef is mefenamate. The results of energy-dispersive spectroscopy (Table 1 and supplementary material) made it possible to identify and quantify the elements present in the samples. The values that were observed were slightly higher than the theoretical values of each element due to the fact that EDS does not identify hydrogen; however, even with this limitation, the values found for all the samples were close to the calculated values.

Thermal analysis

The TG/DTG–DSC curves of the synthesized compounds are shown in Fig. 1. These curves showed that all the compounds were obtained in the anhydrous state and that the thermal decomposition occurred in three overlapping steps in both atmospheres (air and N_2), except for cerium compound where two steps are observed in air atmosphere, which correspond to exothermic (air) or endothermic (N_2) events.

These curves also showed that the thermal stability of the compounds depends on the nature of the metal ion, and they followed the subsequent order:

(air) Nd > La > Pr > Ce (N_2) La > Nd > Ce > Pr

A great similarity was observed in the TG/DTG–DSC curves in air atmosphere of the lanthanum and neodymium compounds, while cerium and praseodymium displayed other TG/DTG–DSC curves, which were characteristic of each compound. On the other hand, in a nitrogen atmosphere, all the TG/DTG–DSC curves were very similar, suggesting that the mechanism of thermal decomposition in an inert atmosphere was quite similar for all compounds.

Table 1 Analytical and thermoanalytical (TG) results for the $Ln(Mef)_3$ compounds

Compound	Ln (oxide)/%				L (lost)/%		C/%			H/%			N/%			Residue
	Calc.	TG	EDTA	EDS[a]	Calc.	TG	Calc.	EA	TG	EDS[a]	Calc.	EA	TG	Calc.	EA	TG	EDS[a]	
$La(Mef)_3$	18.95	19.14	19.17	16.82	81.05	80.86	62.86	62.36	62.71	65.92	4.93	4.81	4.92	4.89	4.79	4.88	6.69	La_2O_3
$Ce(Mef)_3$	19.99	20.19	19.78	17.23	80.01	79.81	62.77	63.12	62.61	65.72	4.93	4.99	4.92	4.88	4.60	4.87	6.99	CeO_2
$Pr(Mef)_3$	19.75	20.09	19.56	16.47	80.25	79.91	62.71	62.57	62.44	65.98	4.92	5.08	4.90	4.88	5.04	4.86	6.96	Pr_6O_{11}
$Nd(Mef)_3$	19.45	19.55	19.68	16.71	80.55	80.45	62.47	62.30	62.39	65.91	4.90	5.01	4.89	4.86	4.70	4.85	6.78	Nd_2O_3

Ln lanthanides, *Mef* mefenamate

[a] The highest percentage difference is due to the fact that the EDS technique does not determine hydrogen

The mass losses (Δm), temperature ranges (θ) and peak temperatures (T_P) observed for each step of the TG/DTG–DSC curves are given in Table 2.

TG/DTG–DSC in air atmosphere

The TG/DTG–DSC curves of the mefenamate compounds are shown in Fig. 1a–d. These curves show that these compounds are thermally stable up to about 325 °C (Nd), 308 °C (La), 302 °C (Pr) and 280 °C (Ce).

For the compounds of lanthanum and neodymium, as shown in Fig. 1a, d, the TG/DTG–DSC curves show that the thermal decomposition occurs in three overlapping steps; the first two corresponded to exothermic peaks, which were attributed to oxidation of the organic matter and/or of the gaseous product that evolved during thermal decomposition. The oxidation of the organic matter yielded an intermediate derivative of carbonate, which was accompanied by a carbonaceous residue. The intermediate probably corresponded to dioxycarbonate ($La_2O_2CO_3$ and $Nd_2O_2CO_3$), as already observed for the complexes of mandelate with light trivalent lanthanides [22]. Tests with hydrochloric acid solution on sample heated to the temperature of formation of this intermediate, as indicated by the corresponding TG/DTG–DSC curves, confirmed the evolution of CO_2 and the presence of the carbonaceous residue. The last step corresponded to a small endothermic peak (La), and no thermal event (Nd) in DSC curves was attributed to the thermal decomposition of derivative of carbonate (endo) together with the oxidation of carbonized residue (exo), which led to the respective oxides (La_2O_3 and Nd_2O_3).

The TG/DTG–DSC curves of cerium mefenamate, as shown in Fig. 1b, showed that the thermal decomposition occurred in a rapid single step, which correspond to a large exothermic peak that was assigned to oxidation of the organic matter and/or of gaseous products evolved during the thermal decomposition, as well as the oxidation reaction of Ce(III) to Ce(IV). However, the DTG curve showed that the thermal decomposition took place in two overlapping steps.

The TG/DTG–DSC curves of praseodymium mefenamate, as shown in Fig. 1c, showed that the thermal decomposition occurred in three overlapping steps, corresponding to two sharp exothermic peaks and a shoulder in the DSC curve attributed to the oxidation of organic matter and/or of the gaseous products evolved during the thermal decomposition and/or the oxidation of Pr(III) to Pr_6O_{11}; these curves did not indicate the formation of a carbonate derivative as a stable intermediate.

TG–DSC/FTIR in air atmosphere

The Gram–Schmidt (GS) curves for all compounds are presented in Fig. 2. The IR spectra selected at different

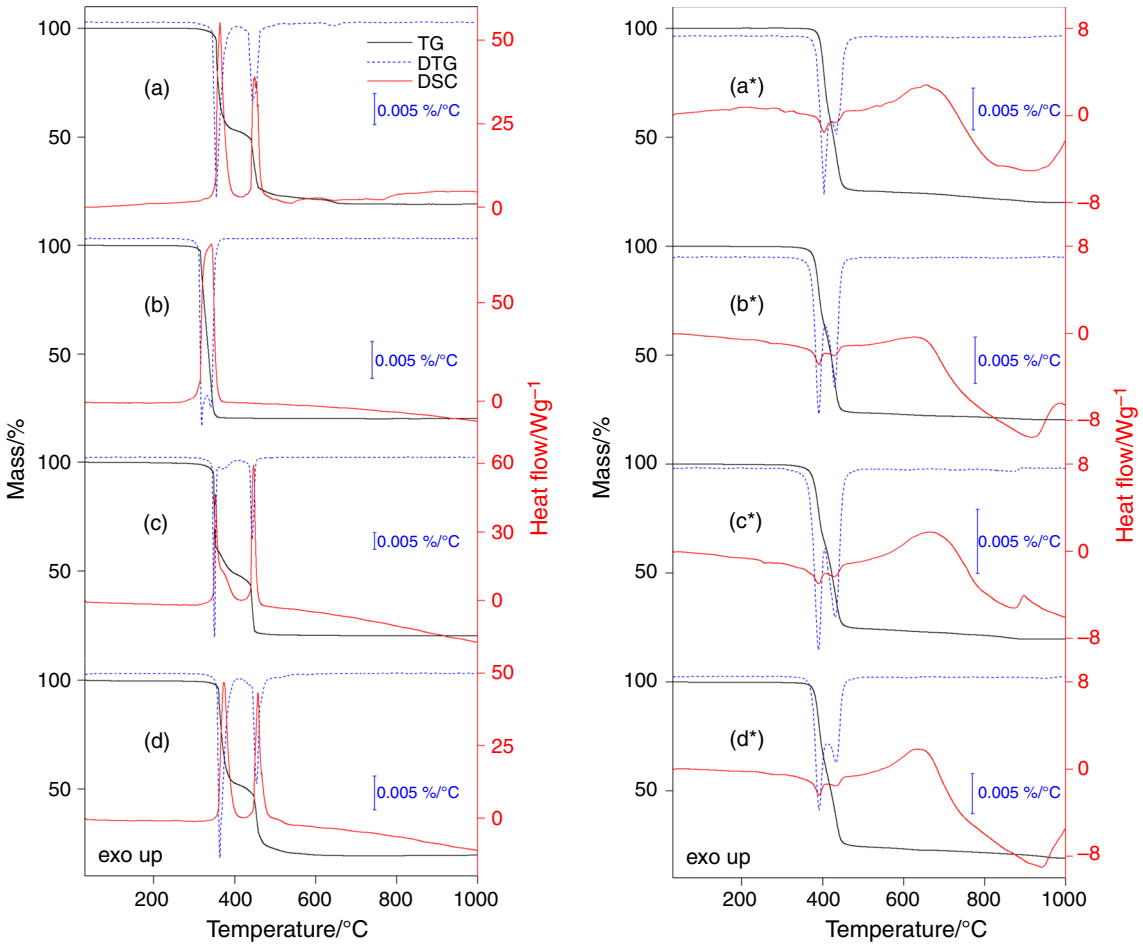

Fig. 1 TG–DSC curves of the compounds in dynamic air atmospheres (*left*): **a** $La(Mef)_3$ (5.015 mg), **b** $Ce(Mef)_3$ (5.066 mg), **c** $Pr(Mef)_3$ (4.993 mg), **d** $Nd(Mef)_3$ (5.019 mg); TG–DSC curves in N_2* atmospheres (*right*): **a*** $La(Mef)_3$ (5.020 mg), **b*** $Ce(Mef)_3$ (5.120 mg), **c*** $Pr(Mef)_3$ (5.114 mg), **d*** $Nd(Mef)_3$ (5.088 mg)

temperatures for the gaseous products that evolved during the thermal decomposition of the lanthanum compound are presented in Fig. 2e, as being representative of all the compounds. They are representative of all the compounds because the gases that were released were the same. The FTIR spectra of the gases released in the thermal decomposition of the other compounds (Ce, Pr and Nd) in selected different temperatures are given in the supplemental material. The GS curves showed no peaks at temperatures below the thermal decomposition onset temperature, suggesting that there was no water of hydration in these compounds. This was also suggested by thermoanalytical (TG/DTG–DSC) and spectroscopic data. For the thermal decomposition steps, the GS curves showed sharp peaks, which were associated with the first and second steps of thermal decomposition of the lanthanum and neodymium mefenamates, the first and third steps for the praseodymium mefenamate; they suggested two overlapping steps for the cerium mefenamate. The last step for the compounds of lanthanum and neodymium and the second for the compound of praseodymium were not clearly observed, probably because the mass losses related to these steps were small (Table 2, a small amount of gas was released) and/or due to the large overlap between the thermal decomposition steps.

Furthermore, based on a library of reference FTIR spectra available in the software of the spectrometer and analysis of the frequency of the vibrational mode, these results allow to suggest which were the main gaseous products released during the thermal decomposition of the compounds. The FTIR spectrum recorded at 360 °C (first step) showed characteristic absorption peaks at 2355 and 2311 cm^{-1}, which were attributed to the stretching asymmetric vibration (ν CO_2) of carbon dioxide molecules. The very weak bands, with peaks in 3425, 3050, 2930, 1588/1500 and 1302 cm^{-1} were assigned to stretching vibrations of the following groups N–H (aromatic secondary amine), C–H (aromatic), C–H (aliphatic), C=C (ring) and C–C [23, 24], respectively, were assigned to the 2,3-dimethyl-N-phenylaniline molecule, confirmed based

Table 2 Temperatures ranges (θ), mass losses (Δm), peak temperatures (T_P) and observed for each step of the TG/DTG–DSC curves of the $Ln(Mef)_3$ compounds

Compounds	Steps						Total Δm	
	First		Second		Third			
	Air	N_2	Air	N_2	Air	N_2	Air	N_2
$La(Mef)_3$								
θ/°C	308–405	360–420	405–500	420–500	500–665	500–920	80.86	80.04
Δm/%	47.23	41.70	29.56	33.00	4.07	5.34		
T_P/°C	362↑	402↓	450↑	430↓	645↓	–		
$Ce(Mef)_3$								
θ/°C	280–331	340–407	331–370	407–460	–	460–910	79.77	79.71
Δm/%	42.19	37.35	37.58	38.77	–	3.59		
T_P/°C	342↑	390↓	342↑	430↓	–	–		
$Pr(Mef)_3$								
θ/°C	302–355	320–405	355–390	405–480	390–500	480–880	79.91	80.37
Δm/%	39.30	36.49	10.89	39.37	29.72	4.51		
T_P/°C	351↑	390↓	370↑, sh	430↓	448↑	–		
$Nd(Mef)_3$								
θ/°C	325–400	350–410	400–480	410–465	445–600	465–960	80.49	80.98
Δm/%	47.38	40.18	29.16	34.72	3.95	6.08		
T_P/°C	372↑	390↓	458↑	435↓	–	–		

sm small; ↑ exo, ↓ endo

on the reference spectra of the diphenylamine and which has a chemical structure very similar to the dimethyl-N-phenylaniline molecule, that was available on the spectrometer program. In the second and third steps of thermal decomposition (400, 445 and 510 °C), only absorption bands of molecules characteristic of CO_2, NH_3 and CO are observed, suggesting the breakdown of the aromatic ring probably due to the combustion of the compound and/or of the 2,3-dimethyl-N-phenylaniline molecules in the phase gas.

TG/DTG–DSC in nitrogen atmosphere

The TG/DTG–DSC curves of the mefenamate compounds are shown in Fig. 1a*–d*. These curves show that these compounds are thermally stable up to about 360 °C (La), 350 °C (Nd), 340 °C (Ce) and 320 °C (Pr).

The thermal decomposition of the compounds from lanthanum and neodymium also occurred in three overlapping steps, as in air atmosphere. However, large differences were observed in the profile of the TG/DTG–DSC curves and increases in thermal stability of the compounds in relation to the thermogravimetric curves that were obtained in air atmosphere, which suggests that the oxidizing atmosphere had a strong influence on the thermal decomposition mechanism. The first and second steps of thermal decomposition which corresponded to two endothermic peaks in the DSC curve were assigned to the thermal decomposition of the compound, which lead to the formation of a mixture of carbonaceous residue with lanthanum and neodymium oxides (La_2O_3 and Nd_2O_3).

For the cerium mefenamate, the thermal stability is much greater than in air atmosphere and the TG/DTG curves showed three mass loss steps, suggesting that the atmosphere has a strong influence on the thermal decomposition mechanism. The first two steps corresponded to two endothermic peaks in the DSC curves and were attributed to thermal decomposition of compound, which lead to the formation of a mixture of carbonaceous residue with cerium oxide (CeO_2).

For the praseodymium mefenamate, the thermoanalytical curves showed that the compound was more stable and the profile of the curves is very different from those curves obtained an oxidant atmosphere, which suggests that the type of atmosphere have a strong influence on the thermal decomposition mechanism. The TG/DTG–DSC curves show that the first two of mass loss steps are well overlapped and corresponded to two endothermic peaks in the DSC which curves attributed to the thermal decomposition of compound, which lead to the formation of a mixture of carbonaceous residue with praseodymium oxide (Pr_6O_{11}).

For all compounds, the last step of mass loss in the TG curve corresponding to an exothermic peak the DSC curve attributed to pyrolysis of carbonized residue and/or the

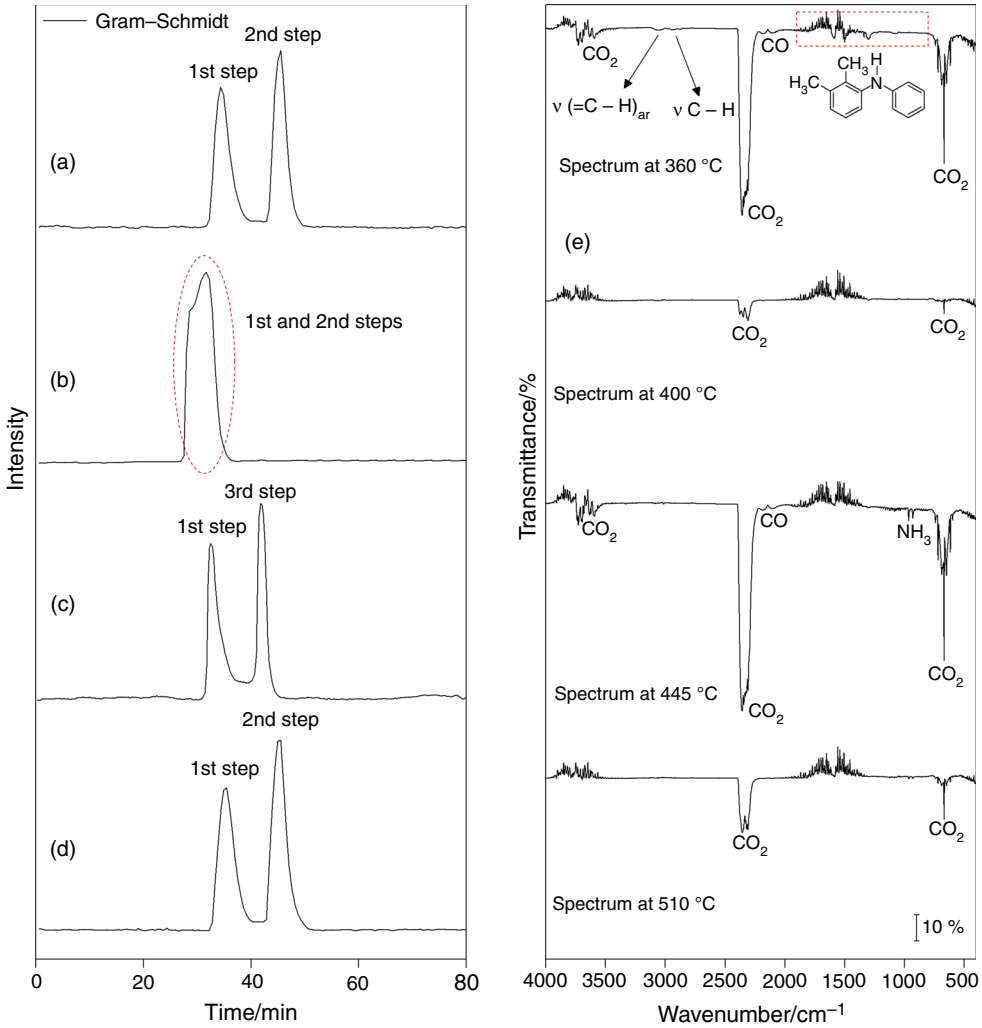

Fig. 2 Gram–Schmidt curves in air atmosphere of the compounds: **a** $La(Mef)_3$, **b** $Ce(Mef)_3$, **c** $Pr(Mef)_3$, **d** $Nd(Mef)_3$ and **e** IR spectra of gaseous products evolved during the thermal decomposition of the lanthanum compound in air atmosphere, as representative of all the compounds

slow oxidation of the carbonized residue, leading to the formation of the respective residues of pure oxides (La_2O_3, CeO_2, Nd_2O_3 and Pr_6O_{11}).

In both atmospheres (air and N_2), the formation of the respective oxides (La_2O_3, CeO_2, Nd_2O_3 and Pr_6O_{11}), as final residue in the thermal decomposition of the compounds in air atmosphere and in N_2 atmosphere, was based on the total mass losses of the TG curves. This was also experimentally verified on the basis on their X-ray diffraction powder patterns.

TG–DSC/FTIR in nitrogen atmosphere

The Gram–Schmidt (GS) curves for all compounds are presented in Fig. 3, and the IR spectra selected at different temperatures for the gaseous products that evolved during the thermal decomposition of the lanthanum compound are presented in Fig. 3e, as being representative of all the compounds. They are representative of all the compounds because the gases that were released were the same. The FTIR spectra of the gases released during the thermal decomposition of the other compounds (Ce, Pr and Nd) at selected different temperatures are contained in the supplemental material. The curves showed that the first and second thermal decomposition steps were well superimposed in accordance with the TG/DTG curves, probably because of the higher thermal stability of the compounds in an inert atmosphere. No sharp peaks were observed in the GS curves during the last step, probably because of the small and slow amount of gases that evolved. Furthermore, based on a library of reference FTIR spectra available in the software of the spectrometer, and analysis of the frequency of the vibrational mode, it was also possible to suggest the main gaseous products during the thermal decomposition of the compounds. With respect to the nature of the gaseous products released during the first two steps of thermal decomposition of the compounds, mainly 2,3-dimethyl-N-phenylaniline and carbon dioxide (CO_2) were identified, suggesting that the main mechanism of thermal decomposition led to the breakdown of the carbon–

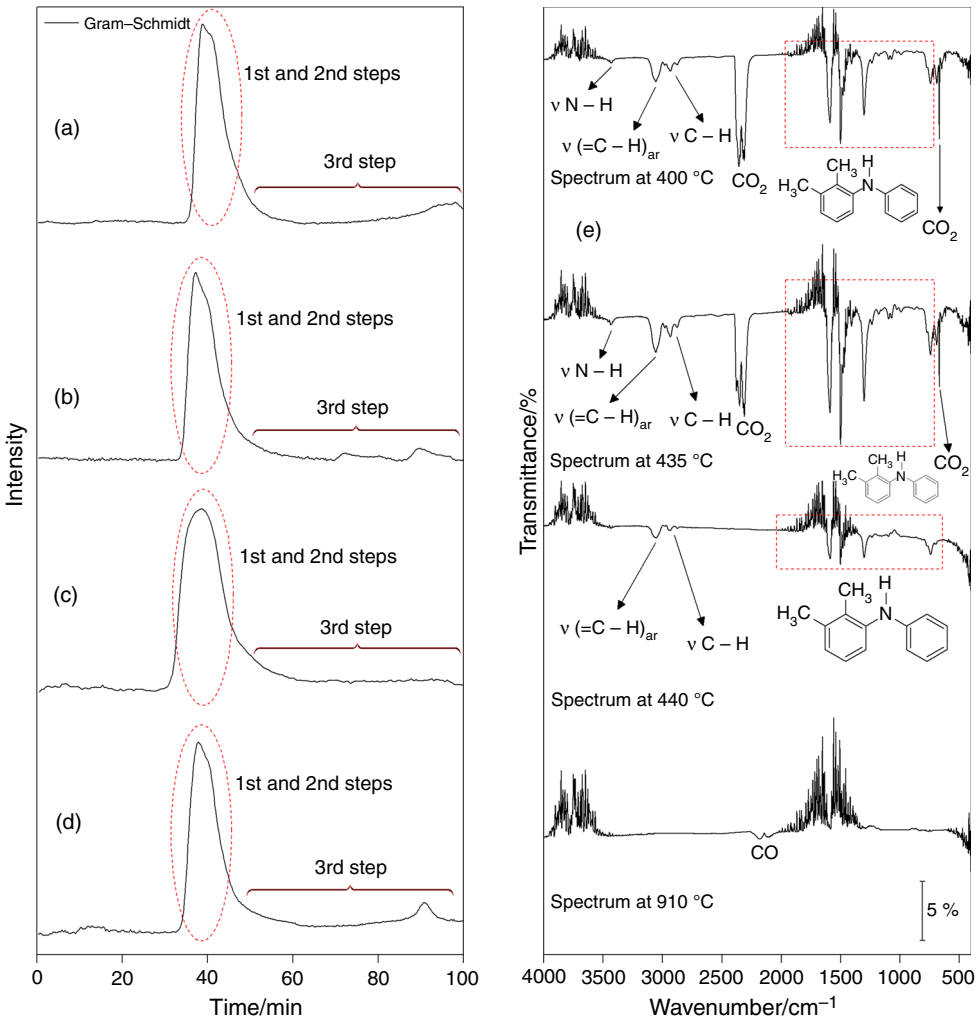

Fig. 3 Gram–Schmidt curves in N_2 atmosphere of the compounds: **a** $La(Mef)_3$, **b** $Ce(Mef)_3$, **c** $Pr(Mef)_3$, **d** $Nd(Mef)_3$ and **e** IR spectra of gaseous products evolved during the thermal decomposition of the lanthanum compound in N_2 atmosphere, as representative of all the compounds

carbon bond of the carboxylate group bound to the aromatic ring. Regarding the last step of mass loss, only carbon monoxide was detected (the characteristic absorption peaks at 2143 cm^{-1} were due to stretching vibration of the C=O group) which was attributed to slow pyrolysis and/or oxidation of the charred residue, due to the presence of oxygen traces.

Interesting observation is that the intensities of the bands of carbon dioxide (CO_2) and 2,3-dimethyl-N-phenylaniline, as shown in Fig. 3 and supplemental material, are different in the stages of thermal decomposition. In the initial stage the bands of CO_2 are more intense than those of the 2,3-dimethyl-N-phenylaniline, but in the second stage the two bands are almost equally intense. In the third stage, the carbon dioxide absorption bands are no longer possible to observe, while the bands of 2,3-dimethyl-N-phenylaniline still appear brightly. This fact is probably due to the size of the two molecules; therefore, with CO_2, less FTIR molecule reaches the detector faster and is therefore drawn or purged to make room for the detection of only 2,3-dimethyl-N-phenylaniline. In the fourth stage, are not observed bands of carbon dioxide nor bands of the 2,3-dimethyl-N-phenylaniline, but observed bands of the carbon monoxide (CO). Thus, it can be suggested that by the low intensity of the bands of carbon monoxide (CO) and the oven temperature high, the substance is a by-product formed by decomposition of 2,3-dimethyl-N-phenylaniline with carbon dioxide. These aspects are different to the compound of cerium due to its faster thermal decomposition; indeed most readily observed under an atmosphere of air, as shown in Fig. 2, it can be suggested that the interaction with the metal binder has a lower intensity than the other compounds.

XRD

The X-ray diffraction powder patterns (see supplementary material) show that all the compounds have crystalline

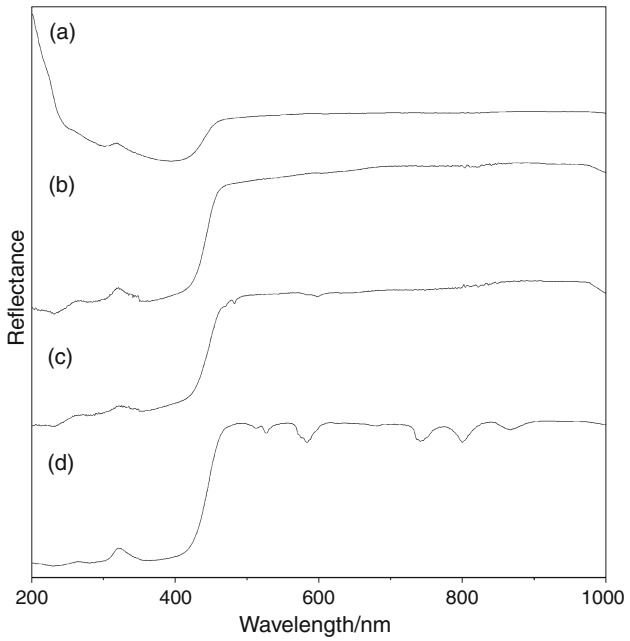

Fig. 4 DR spectra of **a** $La(Mef)_3$, **b** $Ce(Mef)_3$, **c** $Pr(Mef)_3$, **d** $Nd(Mef)_3$

structure and the crystallinity of these compounds followed the order: Pr > Nd > La > Ce. Furthermore, the XRD patterns were very similar, suggesting that the compounds formed an isomorphic series.

Scanning electron microscopy with field emission guns (SEM/FEG)

The micrographs showed that the particles of all the samples had an elongated rectangular shape with dimensions ranging from 1.60 to 25.15 μm^2 (see supplementary material).

DR spectroscopy

The diffuse reflectance (DR) spectra (200–1000 nm) of the Ln^{3+} complexes (Ln = La, Ce, Pr and Nd) containing mefenamic acid are shown in Fig. 4. They exhibited a broad intra-ligand (IL) band in the UV and visible region (200–460 nm). In addition, the spectra of Pr^{3+} and Nd^{3+} also showed the typical absorption bands due to 4*f*–4*f* transitions from the ground states to the excited ones of the Ln^{3+} ions in the 470–1000 nm spectral range. The absorption spectrum of the praseodymium complex showed four peaks, corresponding to the transitions from the $^3H_4$ ground state to the excited states. Characteristic absorption bands were also observed in the spectrum of the neodymium complex. Fourteen peaks were present within this spectral range due to transitions from the $^4I_{9/2}$ ground state to the excited states. These peaks are presented in Table 3 with the assignment of transitions and exhibit shifts in the position compared with the Pr^{3+} and Nd^{3+} free ions [25].

Table 3 Absorption bands of the *f*–*f* transitions in visible and near-infrared regions and covalent parameters of the praseodymium and neodymium compounds

Compounds	Wave number/cm^{-1}	Wavelength/nm	Assignments	Covalent parameters
$Pr(Mef)_3$	21,277	470	$^3H_4 \rightarrow {}^3P_1$	$\beta = 0.9939$
			$^3H_4 \rightarrow {}^1I_6$	$\delta = 0.614$
	20,704	483	$^3H_4 \rightarrow {}^3P_0$	$b^{1/2} = 0.0552$
	17,153, 16,694	583, 599	$^3H_4 \rightarrow {}^1D_2$	
	6976	1433	$^3H_4 \rightarrow {}^3F_4$	
	6590, 6495	1517, 1540	$^3H_4 \rightarrow {}^3F_3$	
	5212, 5137	1919, 1947	$^3H_4 \rightarrow {}^3F_2^a$	
$Nd(Mef)_3$	21,008	476	$^4I_{9/2} \rightarrow {}^2K_{15/2}$	$\beta = 0.9995$
	19,531	512	$^4I_{9/2} \rightarrow {}^4G_{9/2}$	$\delta = 0.050$
	18,975	527	$^4I_{9/2} \rightarrow {}^4G_{7/2}^a$	$b^{1/2} = 0.0158$
	17,361, 17,123	576, 584	$^4I_{9/2} \rightarrow {}^4G_{5/2}^a$	
			$^4I_{9/2} \rightarrow {}^2G_{7/2}$	
	16,051, 15,898	623, 629	$^4I_{9/2} \rightarrow {}^2H_{11/2}$	
	14,684	681	$^4I_{9/2} \rightarrow {}^4F_{9/2}$	
	13,569, 13,495, 13,423, 13,316	737, 741, 745, 751	$^4I_{9/2} \rightarrow {}^4F_{7/2}$	
			$^4I_{9/2} \rightarrow {}^2S_{3/2}$	
	12,500	800	$^4I_{9/2} \rightarrow {}^4F_{5/2}^a$	
			$^4I_{9/2} \rightarrow {}^2H_{9/2}^a$	
	11,547, 11,468	866, 872	$^4I_{9/2} \rightarrow {}^4F_{3/2}$	

[a] Hypersensitive transitions

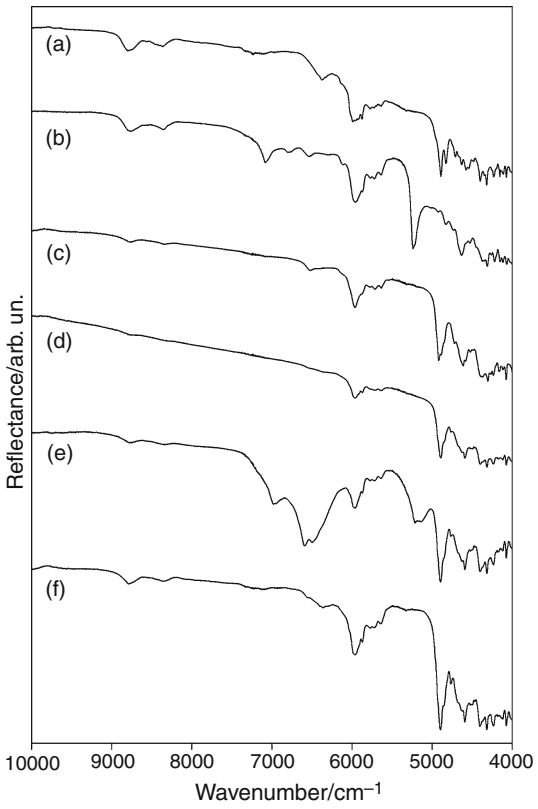

Fig. 5 NIR spectra of **a** HMef, **b** NaMef, **c** $La(Mef)_3$, **d** $Ce(Mef)_3$, **e** $Pr(Mef)_3$, **f** $Nd(Mef)_3$

This shift was related to covalence in metal–ligand bond, and the parameters related to the covalence, Sinha's parameter (δ), nephelauxetic ratio (β) and bonding parameter ($b^{1/2}$) are presented in Table 3. The positive values and the magnitude of these parameters suggest a weak metal–ligand covalent bonding [26].

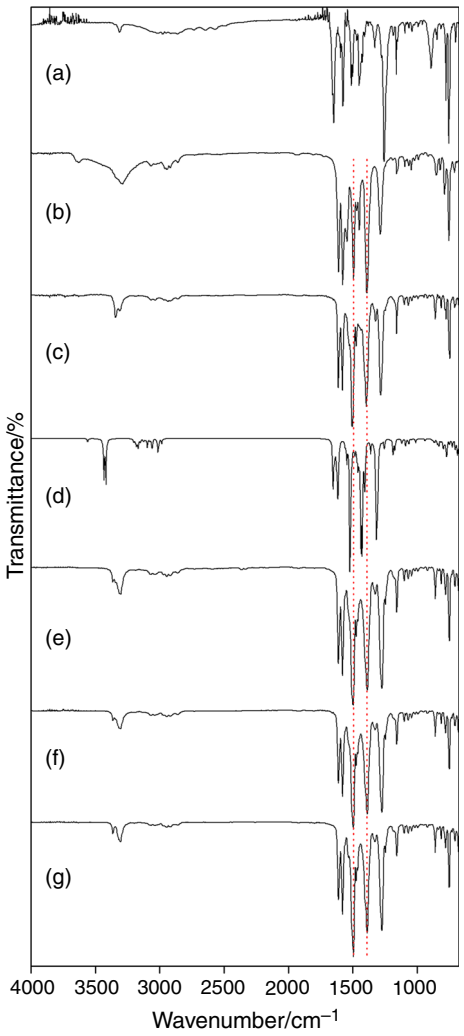

Fig. 6 MIR spectra of **a** HMef, **b** NaMef, **c** $La(Mef)_3$, **d** $La(Mef)_3$ (theoretical), **e** $Ce(Mef)_3$, **f** $Pr(Mef)_3$, **g** $Nd(Mef)_3$

Table 4 Near-infrared bands of the mefenamic acid, sodium salt and lanthanum compounds

Assignment	HMef/cm^{-1}	NaMef/cm^{-1}	$La(Mef)_3$/cm^{-1}
CH_3/CH 2nd overtone bands	8796, 8561, 8361	8768, 8354	8774, 8339
CH_3 1st overtone/combination bands	7236, 7111	7077	7093
CH 1st overtone/combination band	6965	6794	–
NH 1st overtone band	6373	6533	6527
CH_3 1st overtone bands	5987, 5874	6108, 5956, 5869	5958, 5873
CH 1st overtone bands	5772, 5636	5770, 5719, 5636	5771, 5710, 5635
RCO_2H 1st overtone band	5321	–	–
OH_{water} combination bands	–	5236, 5212	–
NH combination bands	4889, 4825, 4709	4921, 4825, 4734	4916, 4888, 4830, 4718
CC combination bands	4630, 4574	4631	4612, 4581
CH_3 combination bands	4541, 4480, 4397, 4345, 4317, 4230	4526, 4369, 4344, 4310, 4258, 4217	4521, 4488, 4388, 4366, 4302, 4264, 4233
CH combination bands	4153, 4110, 4072	4149, 4116, 4065	4164, 4111, 4075

Table 5 Main experimental and theoretical vibrational data (MIR) for the mefenamate (Mef) compounds

Assignments	Frequencies/cm^{-1}				
	Theoretical	Experimental			
	$La(Mef)_3$	$La(Mef)_3$	$Ce(Mef)_3$	$Pr(Mef)_3$	$Nd(Mef)_3$
ν N–H	3557	not observed	–	–	–
ν N–H	3432	3341_w	3362_w	3361_w	3362_w
ν N–H	3416	3310_w	3304_w	3305_w	3305_w
ν $C–H_{ar}$	3201, 3179, 3167, 3150	$(3067, 3032)_{vw}$	$(3068, 3032)_{vw}$	$(3067, 3039)_{vw}$	$(3068, 3036)_{vw}$
ν $C–H_{(methyl\ groups)}$	3096, 3076, 3057, 3012, 2982	$(2967, 2935, 2918, 2859)_{vw}$	$(2970, 2944, 2917, 2861)_{vw}$	$(2968, 2945, 2916, 2861)_{vw}$	$(2972, 2946, 2916, 2858)_{vw}$
ν $C=C_{ring}$ + δ $C–H_{ar}$ + δ N–H	1653, 1616	$1613, 1580_s$	$1613_s, 1580_s$	$1612_s, 1580_s$	$1612_s, 1580_s$
ν $C=C_{ring}$ + δ $C–H_{ar}$ + δ N–H + ν $C–H_{(methyl\ groups)}$	1545	1527_w	1530_{sh}	1530_{sh}	1533_w
ν_{as} COO^- + ν $C=C_{ring}$ + δ $C–H_{ar}$ + ν $C–H_{(methyl\ groups)}$	1523	1505_{vs}	1497_{vs}	1495_{vs}	1495_{vs}
ν_s $COO^-(1)$ + δ $C–H_{ar}$ + δ N–H	1425	1396_{vs}	1387_{vs}	1388_{vs}	1388_{vs}
ν C–N + δ $C–H_{ar}$	1317	1284_s	1273_s	1273_{vs}	1273_{vs}

vs very strong, *s* strong, *w* weak, *vw* very weak, *sh* shoulder

ν stretching vibrations, vas (COO^-) antisymmetric carboxyl stretching frequency, vs (COO^-) symmetric carboxyl stretching frequency, *δ* bending vibration

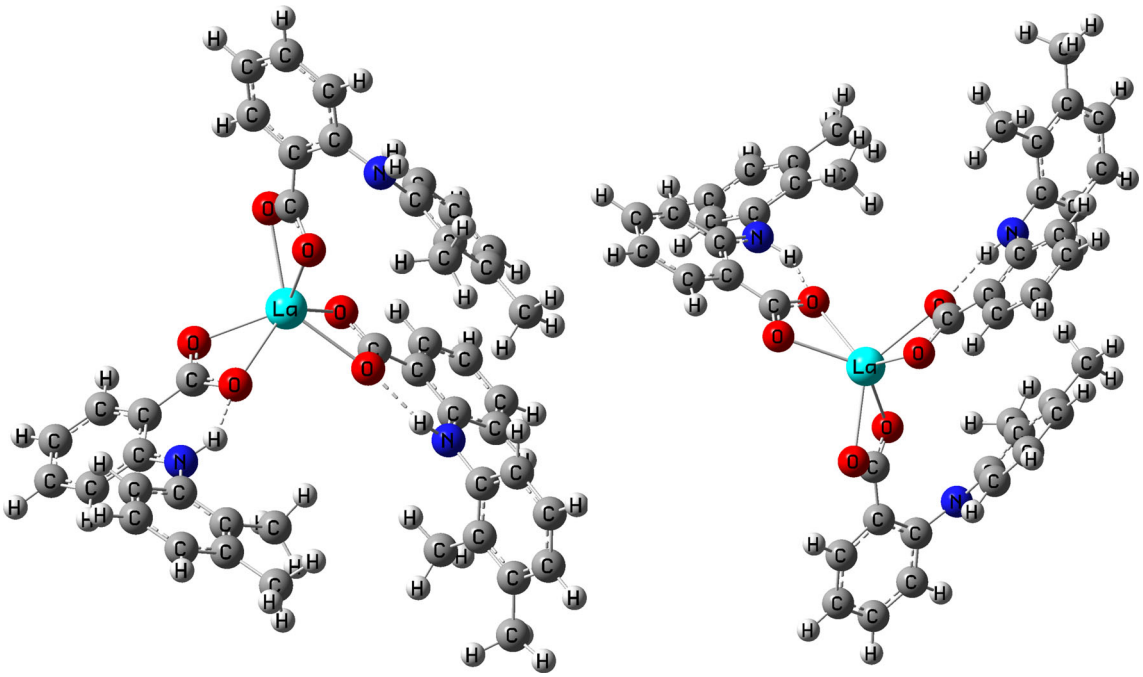

Fig. 7 Theoretical 3D structure of $La(Mef)_3$ compound

NIR spectroscopy

The near-infrared (NIR) spectra of mefenamic acid, sodium salt of mefenamic acid and lanthanum compounds are shown in Fig. 5. The assignments of the bands are shown in Table 4 for the acid form, the sodium salt and the lanthanum compound. For the other complexes, the assignment of the bands was the same to the lanthanum, differing only for the praseodymium complex, which exhibited bands that were assigned to *f–f* transitions (shown in Table 3). Characteristic water bands only appeared in the sodium salt, in agreement with the TG–DSC results.

Characteristic bands of carboxylic acid only appeared in the acid form, confirming the total deprotonation and the absence of acid contamination in the sodium salt and in the complexes.

MIR spectroscopy and theoretical calculation

The infrared spectroscopic spectra of the mefenamic acid, sodium salt and the lanthanide mefenamates are shown in Fig. 6, and the most important IR frequencies (theoretical and experimental) of the mefenamate compounds along with their assignments are presented in Table 5; the experimental values were determined based on the theoretical calculation and references [23, 24]. As can be seen, there was a great similarity between the experimental and theoretical spectrum, which suggests that the lanthanum compound had the structure as shown in Fig. 7, from whence the theoretical infrared spectrum was generated; the great similarity between the spectra suggests that all the compounds are coordinated in the same way. On the other hand, a large similarity between the spectra of the compounds and the sodium salt is observed, especially in values of the frequencies associated with the vibrations of the carboxylate group—the coordination site for the metals—which suggests a large ionic character of these compound bonds; this was also suggested by other spectroscopic data (Table 3). Another interesting fact refers to bands assigned to the stretching vibration of the amine group (ν N–H), where two bands were observed in the spectra of the compounds in the region between 3362 and 3304 cm^{-1}. This was also observed in the free ligand (mefenamic acid) [27], which is associated with the two polymorphic forms of mefenamic acid. The first, around 3311 cm^{-1}, refers to form I, where the hydrogen participates in hydrogen bonding with the carboxylic group, and the second around 3345 cm^{-1}, refers to form II, where there is no hydrogen bonding with the carboxylic group. These observations suggest that there should have been similar interactions in the lanthanide compounds in agreement with the calculated (Fig. 7), and also, as observed in other compounds [28, 29].

Conclusions

Using TG, complexometry, EA results and energy-dispersive spectroscopy, a general formula was established for the synthesized compounds: $Ln(Mef)_3$.

The simultaneous TG/DTG–DSC data provided previously unreported information about the thermal stability and thermal decomposition of these compounds in dynamic air and nitrogen atmospheres.

The thermal decomposition of the compounds analyzed in this work by using a TG–DSC/FTIR system for analysis of the gaseous products resulted in the release of 2,3-dimethyl-N-phenylaniline, ammonia, CO and CO_2 in air atmosphere and 2,3-dimethyl-N-phenylaniline, CO and CO_2 in N_2 atmosphere.

The experimental spectroscopic mid-infrared region data and the theoretical calculations suggest that the binding of the mefenamate to the lanthanide (III) ions is performed in a bidentate mode through the carboxylate group. The similarity between the experimental infrared spectra suggests that all the compounds are coordinated in a similar way.

The DR spectra provide information about the ligand absorption bands and the *f–f* transitions of Nd^{3+} and Pr^{3+} ions. The shifts in these bands, compared to the free ions, indicated a weak metal–ligand covalent bonding. Praseodymium also shows *f–f* transitions in NIR region.

Acknowledgements The authors thank FAPESP, CNPq and CAPES Foundations (Brazil) for financial support. This research was supported by resources supplied by the Center for Scientific Computing (NCC/Grid UNESP) of the São Paulo State University (UNESP), Instituto de Quimica de Araraquara, UNESP Campus de Araraquara and CENAPAD-UNICAMP.

References

1. Campos FX, Soares MRS, Terezo AJ, Siqueira AB. Synthesis, characterization, and antioxidant evaluation of solid-state mefenamates of some bivalent metals. J Therm Anal Calorim. 2014;115:167–76.
2. Feng J, Du X, Liu H, Sui X, Zhang C, Tang Y, Zhang J. Manganese-mefenamic acid complexes exhibit high lipoxygenase inhibitory activity. Dalton Trans. 2014;43:10930–9.
3. Dimiza F, Papadopoulos AN, Tangoulis V, Psycharis V, Raptopoulou CP, Kessissoglou DP, Psomas G. Biological evaluation of non-steroidal anti-inflammatory drugs-cobalt(II). Dalton Trans. 2010;39:4517–28.
4. Andrews PC, Franck R, Junk PC, Kedzierski L, Kumar I, MacLellan JG. Anti-Leishmanial activity of homo-and heteroleptitic bismuth (III) carboxylates. J Inorg Biochem. 2010;105:454–61.
5. Tarushi A, Karaflou Z, Klju J, Turel I, Psomas G, Papadopoulos AN, Kessissoglou D. Antioxidant capacity and DNA-interaction studies of zinc complexes with a non-steroidal anti-inflammatory drug, mefenamic acid. J Inorg Biochem. 2013;128:85–96.
6. Brzyska W, Ozga W. Thermal decomposition of yttrium and lanthanide complexes with mephenamic acid. Thermochim Acta. 1992;195:149–55.
7. Bojarowicz H, Kokot Z, Surdykowski A. Complexes of Fe(III) ions with mefenâmico acid. J Pharm Biomed Anal. 1996;15:339–42.
8. Gálico DA, Holanda BB, Perpétuo GL, Schnitzler E, Treu-Filho O, Bannach G. Thermal and spectroscopic studies on solid ketoprofen of lighter trivalent lanthanides. J Therm Anal Calorim. 2012;108:371–9.
9. Gálico DA, Guerra RB, Perpétuo GL, Santos LS, Schnitzler E, Bannach G. Braz J Therm Anal. 2012;1:46–51.
10. Gálico DA, Lahoud MG, Davolos MR, Frem RCG. Fraga-SilvaTFC, Venturini J, Arruda MSP, Bannach G. Spectroscopic, luminescence and in vitro biological studies of heavier trivalent lanthanides and yttrium (III). J Inorg Biochem. 2014;140:160–6.

11. Flaschka HA. EDTA titrations. 1st ed. Oxford: Pergamon Press; 1964.
12. Ionashiro M, Graner CAF, Zuanon Netto J. Titulação complexometria de lantanídeos e ítrio. Ecl Quim. 1983;8:29–32.
13. Becke AD. Density-functional thermochemistry. 3. The role of exact exchange. J Chem Phys. 1993;98:5648–52.
14. Lee C, Yang W, Parr RG. Development of the colle-salvetti correlation-energy formula into a functional of the electrondensity. Phys Rev B. 1988;37:785–9.
15. Filho OT, Pinheiro JC, Costa EB, Ferreira JEV, Figueiredo AF, Kondo RT, Lucca Neto VA, Souza RA, Legendre OA, Mauro AE. Experimental and theoretical study of the compound [Pd(dmba)(NCO)(imz)]. J Mol Struct. 2007;829:195–201.
16. Filho OT, Pinheiro JC, Kondo RT, Marques RFC, Paiva-Santos CO, Davolos MR, Jafelicci M Jr. Gaussian basis sets to the theoretical study of the electronic structure of perovskite ($LaMnO_3$). J Mol Struct (Theochem). 2003;631:93–9.
17. Filho OT, Pinheiro JC, Kondo RT. Designing Gaussian basis sets to the theoretical study of the piezoelectric effect of perovskite ($BaTiO_3$). J Mol Struct. 2004;671:71–5.
18. Frisch MJ, Trucks GW, Schlegel HB, Scuseria GE, Robb MA, Cheeseman JR, Scalmani G, Barone V, Mennucci B, Petersson GA, Nakatsuji H, Caricato M, Li X, Hratchian HP, Izmaylov AF, Bloino J, Zheng G, Sonnenberg JL, Hada M, Ehara M, Toyota K, Fukuda R, Hasegawa J, Ishida M, Nakajima T, Honda Y, Kitao O, Nakai H, Vreven T, Jr. Montgomery JA, Peralta JE, Ogliaro F, Bearpark M, Heyd JJ, Brothers E, Kudin KN, Staroverov VN, Kobayashi R, Normand J, Raghavachari K, Rendell A, Burant JC, Iyengar SS, Tomasi J, Cossi M, Rega N, Millam NJ, Klene M, Knox JE, Cross JB, Bakken V, Adamo C, Jaramillo J, Gomperts R, Stratmann RE, Yazyev O, Austin AJ, Cammi R, Pomelli C, Ochterski JW, Martin RL, Morokuma K, Zakrzewski VG, Voth GA, Salvador P, Dannenberg JJ, Dapprich S, Daniels AD, Farkas O, Foresman JB, Ortiz JV, Cioslowski J, Fox DJ. Gaussian 09, Revision A.02 Inc. Wallingford, CT, 2009.
19. Goodson DZ, Sarpal SK, Wolfsberg M. Influence on isotope effect calculations of the method of obtaining force constants from vibrational data. J Phys Chem. 1982;86:659–63.
20. Schelegel HB. In: Bertran J, editor. New theoretical concepts for understanding organic reactions. Dordrecht: Kluwer Academic Publishers; 1989. p. 33–53.
21. Dennington R, Keith T, Millam J. GaussView, Version 5.0.8, Semichem Inc. Shawnee Mission, KS, 2000–2008.
22. Locatelli JR, Caires FJ, Ionashiro EY, Carvalho CT. Synthesis, Characterization and Thermal Behavior of Solid-State Compounds of Light Trivalent Lanthanide Malonates. Braz. J. Therm. Anal. 2013;2(1):23–30.
23. Socrates G. Infrared characteristic group frequencies. vol. 91, 2nd ed. New York: Wiley; 1994.
24. Silverstein RM, Webster FX. Spectrometric identification of organic compounds. 6th ed. New York: Wiley; 1988.
25. Sastri VS, Bünzli JCG, Rao VR, Rayudu GVS, Perumareddi JR. Modern aspects of rare earths and their complexes. Amsterdam: Elsevier; 2003.
26. Iftikhar K, Sayeed M, Ahmad N. Lanthanoid shift reagents. Synthesis and spectral studies. Bull Chem Soc Jpn. 1982;55:2258–63.
27. Gilpin RK, Zhou W. Infrared studies of the polymorphic states of the fenamates. J Pharm Biomed Anal. 2005;37:509–15.
28. Totta X, Papadopoulou AA, Hatzidimitriou AG, Papadopoulos A, Psomas G. Synthesis, structure and biological activity of nickel (II) complexes with mefenamate and nitrogen-donor ligands. J Inorg Biochem. 2015;145:79–93.
29. Tabrizi L, Chiniforoshan H, Mcardle P. A cobalt (II) complex with anionic and neutral N-donor ligands: synthesis, crystal structure, and application as a heterogeneous catalyst for olefin epoxidation with tert-BuOOH. J Coord Chem. 2015;68:980–92.